

# Supplementary Material for *Turbulent-like flows in quasi two-dimensional dense sus- pensions of motile colloids*

Rui Luo<sup>1</sup>, Alexey Snezhko<sup>2</sup>, and Petia M. Vlahovska<sup>1</sup>

## 1 Isolated Quincke Random Walker

The speed of an isolated Quincke random walker takes time to reach a steady state. At  $E = 1.7E_q$ , the speed eventually stabilizes to a steady state. However, at  $E = 4.6E_q$ , the particle's speed exhibits oscillations with a larger amplitude when the field is applied, and it continues to increase throughout the runtime  $\tau_{\text{on}}$ .

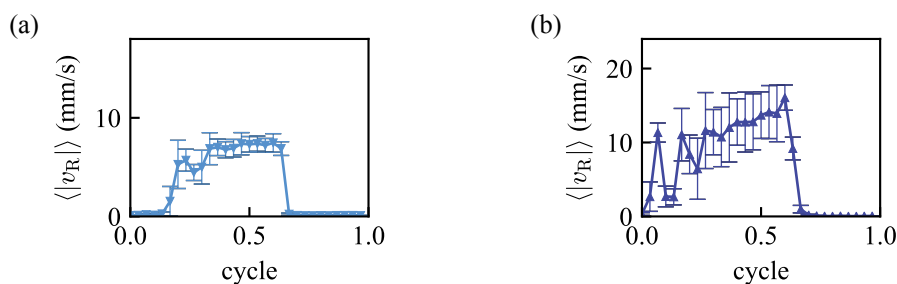


Figure 1: Speed measurements of an isolated Quincke random walker at different field strengths: (a)  $E = 1.7E_q$  and (b)  $E = 4.6E_q$ . The data represent averages over 10 cycles for an isolated particle. Error bars indicate the standard deviation of the measured speed.

## 2 Experimental Imaging and Analysis Methods

### 2.1 Imaging Setup and Parameters

For imaging, a high-speed camera (Photron SA 1.1) is employed in conjunction with a microscopy setup (Zeiss, 2x magnification). The frame rate (fps) is strategically selected to be either 500 or 1000, depending on the particle concentration and the applied field strength. This selection ensures that the motion of the particles is adequately resolved, facilitating accurate tracking and analysis of their dynamics under the experimental conditions.

### 2.2 Velocity and Vorticity Measurements

#### 2.2.1 Dilute Suspensions: Particle Tracking Velocimetry (PTV)

In dilute suspensions (area fraction  $\phi < 0.4$ ), Particle Tracking Velocimetry (PTV) is employed to measure individual particle velocities. The Trackpy[1] library is utilized for this purpose. When dealing with images captured at different frame rates (fps) under varying field strengths or concentrations, the time interval used to link particles is carefully chosen such that the displacement of particles between frames remains within 1/4 to 1/2 of the particle diameter. This ensures accurate tracking without excessive ambiguity or loss of particles due to large displacements. The flow field is then reconstructed using cubic interpolation of the scattered particle data points to generate interpolated velocity values on

<sup>1</sup>Engineering Sciences and Applied Mathematics, Northwestern University, Evanston, IL 60208, USA. E-mail: petia.vlahovska@northwestern.edu

<sup>2</sup>Materials Science Division, Argonne National Laboratory, 9700 South Cass Avenue, Lemont, Illinois 60439, USA.

a predefined grid. This interpolation is facilitated by the `scipy.interpolate.griddata` function with the `cubic(2D)` method.

### 2.2.2 Dense Suspensions: Particle Image Velocimetry (PIV)

For dense suspensions with an area fraction of particles  $\phi \geq 0.5$ , the suspension is treated as a continuum phase. In this regime, Particle Image Velocimetry (PIV) is utilized to determine the velocity field. The OpenPIV[3] library in Python is employed to estimate the 2D velocity field on a 2D cubic grid. Averaging windows of size 20 pixels by 20 pixels are selected, corresponding approximately to 2 by 2 times the mean particle diameter of  $100 \mu\text{m}$  for Polymethyl methacrylate (PMMA) particles. This window size ensures statistical reliability while resolving spatial flow field structures on the order of a few bacterial lengths. A 50% overlap between neighboring bins is used to enhance spatial resolution and accuracy.

### 2.2.3 Vorticity Calculation

The vorticity of the flow is computed using a second-order central difference scheme, implemented through the `numpy.gradient` function, which calculates the spatial derivatives required for vorticity determination. The results were cross-validated using Richardson's Extrapolation (four-point central), confirming consistency.

## 2.3 Energy Spectra Calculation

The total kinetic energy (per unit mass) of a 2D system is defined in real space as:

$$E = \frac{1}{2} \int_{\mathbb{R}^2} \mathbf{v}(\mathbf{r}) \cdot \mathbf{v}(\mathbf{r}) d\mathbf{r}. \quad (1)$$

To analyze spectral energy distribution, we express the velocity field through its Fourier transform,

$$\mathbf{v}(\mathbf{r}) = \frac{1}{(2\pi)^2} \int_{\mathbf{k}} \hat{\mathbf{v}}(\mathbf{k}) e^{i\mathbf{k} \cdot \mathbf{r}} d\mathbf{k}, \quad (2)$$

where the Fourier coefficients are given by,

$$\hat{\mathbf{v}}(\mathbf{k}) = \int_{\mathbb{R}^2} \mathbf{v}(\mathbf{r}) e^{-i\mathbf{k} \cdot \mathbf{r}} d\mathbf{r}. \quad (3)$$

Relating

$$\begin{aligned} \int_{\mathbf{k}} \hat{\mathbf{v}}(\mathbf{k}) \cdot \hat{\mathbf{v}}^*(\mathbf{k}) d\mathbf{k} &= \int_{\mathbf{k}} \int_{\mathbb{R}^2} \int_{\mathbb{R}^2} \mathbf{v}(\mathbf{r}) \cdot \mathbf{v}(\mathbf{r}') e^{-i\mathbf{k} \cdot (\mathbf{r}' - \mathbf{r})} d\mathbf{r} d\mathbf{r}' d\mathbf{k} \\ &= \int_{\mathbb{R}^2} \int_{\mathbb{R}^2} \mathbf{v}(\mathbf{r}) \cdot \mathbf{v}(\mathbf{r}') \int_{\mathbf{k}} e^{-i\mathbf{k} \cdot (\mathbf{r}' - \mathbf{r})} d\mathbf{k} d\mathbf{r} d\mathbf{r}' \\ &= (2\pi)^2 \int_{\mathbb{R}^2} \int_{\mathbb{R}^2} \mathbf{v}(\mathbf{r}) \cdot \mathbf{v}(\mathbf{r}') \delta(\mathbf{r}' - \mathbf{r}) d\mathbf{r} d\mathbf{r}' \\ &= (2\pi)^2 \int_{\mathbb{R}^2} \mathbf{v}(\mathbf{r}) \cdot \mathbf{v}(\mathbf{r}) d\mathbf{r}, \end{aligned} \quad (4)$$

using the orthogonality of Fourier modes,

$$\int_{\mathbf{k}} e^{-i\mathbf{k} \cdot (\mathbf{r}' - \mathbf{r})} d\mathbf{k} = (2\pi)^2 \delta(\mathbf{r}' - \mathbf{r}), \quad (5)$$

we simplify to,

$$E = \frac{1}{2(2\pi)^2} \int_{\mathbf{k}} |\hat{\mathbf{v}}(\mathbf{k})|^2 d\mathbf{k}. \quad (6)$$

To derive the radial energy spectrum  $E(k)$ , we convert to polar coordinates  $(k, \theta)$  and average over angular dependence:

$$E = \frac{1}{2(2\pi)^2} \int_0^\infty k \left( \int_0^{2\pi} |\hat{\mathbf{v}}(k, \theta)|^2 d\theta \right) dk. \quad (7)$$

For homogeneous isotropic turbulence, the energy depends only on wavenumber magnitude  $k$ . Defining the angle-averaged power spectrum,

$$\langle |\hat{\mathbf{v}}(k)|^2 \rangle_\theta = \frac{1}{2\pi} \int_0^{2\pi} |\hat{\mathbf{v}}(k, \theta)|^2 d\theta, \quad (8)$$

we obtain the energy spectrum,

$$E(k) = \frac{k}{4\pi L^2} \langle |\hat{\mathbf{v}}(k)|^2 \rangle_\theta, \quad (9)$$

which satisfies  $E = L^2 \int_0^\infty E(k) dk$  and  $L^2$  is the area.

### 2.3.1 Wiener-Khinchin Theorem

The energy spectrum can alternatively be computed from the velocity correlation function  $C_{vv}(\mathbf{R}) = \langle \mathbf{v}(\mathbf{r}) \cdot \mathbf{v}(\mathbf{r} + \mathbf{R}) \rangle_{\mathbf{r}}$  via the Wiener-Khinchin theorem[2],

$$\frac{|\hat{\mathbf{v}}(\mathbf{k})|^2}{(2\pi)^2} = \int C_{vv}(\mathbf{R}) e^{-i\mathbf{k} \cdot \mathbf{R}} d\mathbf{R}. \quad (10)$$

Substituting into the expression for  $E(k)$ ,

$$E(k) = \frac{\pi}{A} k \left\langle \int C_{vv}(\mathbf{R}) e^{-i\mathbf{k} \cdot \mathbf{R}} d\mathbf{R} \right\rangle_\theta, \quad (11)$$

where  $\langle \cdot \rangle_\theta$  indicates averaging over the direction of  $\mathbf{k}$  (azimuthal angle  $\theta$ ).

### 2.3.2 FFT and Windowing Effect

The derivation in 2.3.1 used Wiener-Khinchin theorem to relate the energy spectrum with velocity spatial correlation function, which is valid in infinite domain. Our experiment is neither infinite nor periodic. The discontinuity of the boundary could effect the energy spectrum. We use a Hanning window[4] to process the velocity field measured from experiment, before computing energy spectrum directly (Eq. 9) or from correlation function (Eq. 11). The Hanning window is defines as  $w(x, y) = \frac{1}{4} [1 - \cos(2\pi x/L)] [1 - \cos(2\pi y/L)]$ .  $L$  is the size of the square region of velocity field. We would like to point out the result difference from no windowing procedure and correlation equation (Eq. 11), which shows the error of energy spectrum result without dealing with the in-continuous and non-periodic experimental data. In the main test, we use the direct method (Eq. 9).

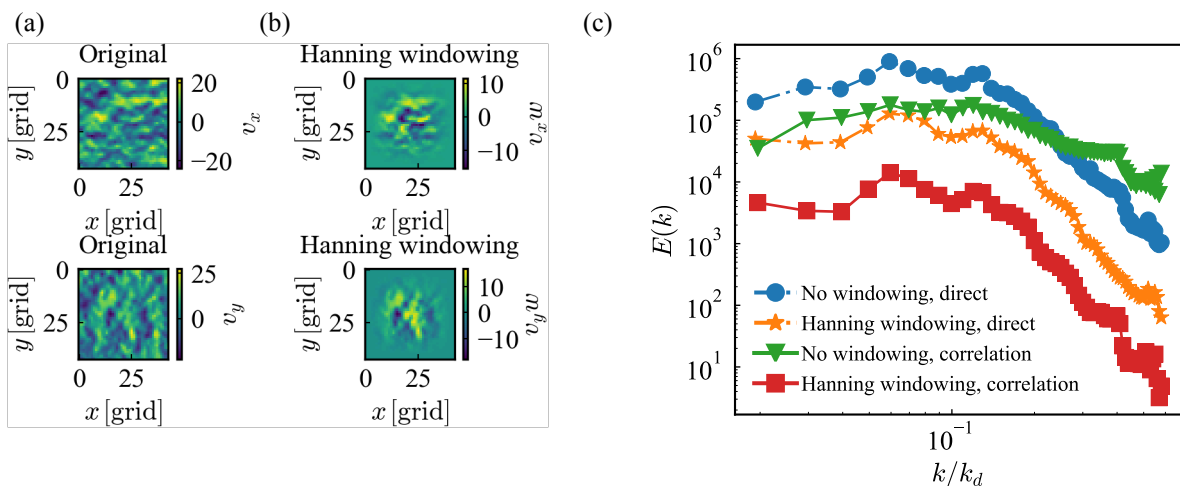


Figure 2: (a) Original velocity field based on PIV. (b) Velocity field after applying Hanning window. (c) Comparison of the energy spectrum based on direct method or correlation function.

## 2.4 Concentration effect on temporal anti-correlation strength

$AE = 2.8 \text{ V}/\mu\text{m}$ , reducing the concentration from  $\phi = 0.82$  to  $\phi = 0.70$  first strengthens and then weakens the anti-correlation (Figure 1), indicating a non-monotonic dependence on concentration. This suggests that the persistence of the anti-correlation is influenced by both field strength and concentration—possibly mediated by persistence length—though further study is needed for a complete understanding.

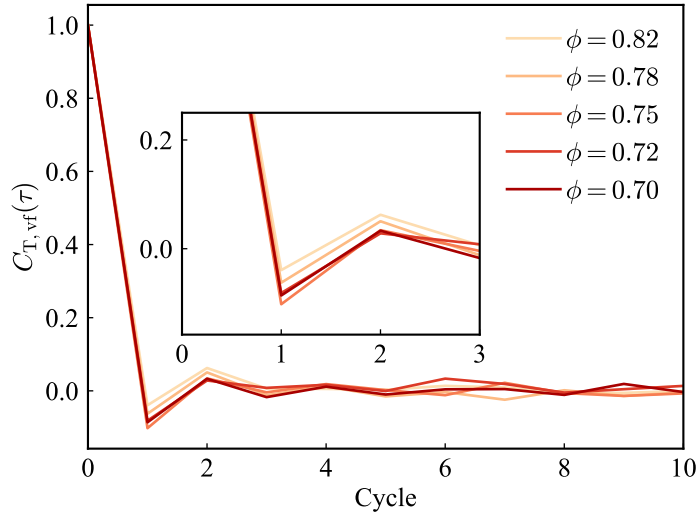


Figure 3: Non-monotonic dependence of the anti-correlation strength on particle concentration. The inset provides a zoomed-in view of the anti-correlation region.

## 3 Movies

The black boundaries in all movies are visual aids, not physical barriers. The Quincke random walkers are driven by a pulsating electric field of fixed frequency ( $\tau_{\text{on}} = 40 \text{ ms}$ ,  $\tau_{\text{off}} = 20 \text{ ms}$ ).

- SI Movie 1: Isolated Quincke random walker. The particle diameter is  $100 \mu\text{m}$ . The field strength is  $4.4 \text{ V}/\mu\text{m}$ .
- SI Movie 2: Turbulent-like flow pattern of Quincke random walkers at high field strength, high concentration. The fields strength  $E$  is  $7.4 \text{ V}/\mu\text{m}$ . The particle area fraction  $\phi_i$  is 0.66.
- SI Movie 3: Turbulent-like flow pattern of Quincke random walkers at low field strength, low concentration. The fields strength  $E$  is  $2.8 \text{ V}/\mu\text{m}$ . The particle area fraction  $\phi_i$  is 0.27.

## References

- [1] Daniel B. Allan, Thomas Caswell, Nathan C. Keim, Casper M. van der Wel, and Ruben W. Verweij. *Soft-matter/trackpy: V0.6.4*. Zenodo, July 2024.
- [2] Uriel Frisch. *Turbulence: The Legacy of A. N. Kolmogorov*. Cambridge University Press, 1995.
- [3] Alex Liberzon, Theo Käufer, Andreas Bauer, Peter Vennemann, and Erich Zimmer. *OpenPIV/openpiv-python: OpenPIV-python v0.23.4*. Zenodo, January 2021.
- [4] Sam Wilken, Rodrigo E. Guerra, David J. Pine, and Paul M. Chaikin. Hyperuniform Structures Formed by Shearing Colloidal Suspensions. *Physical Review Letters*, 125(14):148001, September 2020.